





## Reproductive endocrinology

# Human ovarian aging is characterized by oxidative damage and mitochondrial dysfunction

Myrthe A.J. Smits <sup>1,2</sup>, Bauke V. Schomakers<sup>3,4</sup>, Michel van Weeghel<sup>3,4</sup>, Eric J.M. Wever<sup>3,4</sup>, Rob C.I. Wüst<sup>5,6</sup>, Frederike Dijk<sup>7</sup>, Georges E. Janssens<sup>3,8</sup>, Mariëtte Goddijn<sup>2,9</sup>, Sebastiaan Mastenbroek <sup>1,2,\*</sup>, Riekelt H. Houtkooper <sup>3,8,10,\*</sup>, and Geert Hamer <sup>1,2,\*</sup>

<sup>1</sup>Reproductive Biology Laboratory, Center for Reproductive Medicine, Amsterdam UMC location University of Amsterdam, Amsterdam, The Netherlands

<sup>2</sup>Amsterdam Reproduction and Development Research Institute, Amsterdam, The Netherlands

<sup>3</sup>Laboratory Genetic Metabolic Diseases, Amsterdam UMC location University of Amsterdam, Amsterdam, The Netherlands

<sup>4</sup>Core Facility Metabolomics, Amsterdam UMC, University of Amsterdam, Amsterdam, The Netherlands

<sup>5</sup>Laboratory for Myology, Department of Human Movement Sciences, Faculty of Behavioural and Movement Sciences, Vrije Universiteit Amsterdam, Amsterdam, The Netherlands




<sup>6</sup>Amsterdam Movement Sciences, Amsterdam, The Netherlands

<sup>7</sup>Department of Pathology, Cancer Center Amsterdam, Amsterdam UMC, University of Amsterdam, Amsterdam, The Netherlands

<sup>8</sup>Amsterdam Gastroenterology, Endocrinology, and Metabolism, Amsterdam, The Netherlands

<sup>9</sup>Center for Reproductive Medicine, Amsterdam UMC location University of Amsterdam, Amsterdam, The Netherlands

<sup>10</sup>Amsterdam Cardiovascular Sciences, Amsterdam, The Netherlands

\*Correspondence address. Reproductive Biology Laboratory, Center for Reproductive Medicine, Amsterdam UMC location University of Amsterdam, Meibergdreef 9, 1105 AZ Amsterdam, The Netherlands. E-mail: s.mastenbroek@amsterdamumc.nl  <https://orcid.org/0000-0002-7550-2924> (S.M.); Laboratory Genetic Metabolic Diseases, Amsterdam UMC location University of Amsterdam, Meibergdreef 9, 1105 AZ Amsterdam, The Netherlands. E-mail: r.h.houtkooper@amsterdamumc.nl  <https://orcid.org/0000-0001-9961-0842> (R.H.H.); Reproductive Biology Laboratory, Center for Reproductive Medicine, Amsterdam UMC location University of Amsterdam, Meibergdreef 9, 1105 AZ Amsterdam, The Netherlands. E-mail: g.hamer@amsterdamumc.nl  <https://orcid.org/0000-0002-9583-6796> (G.H.)

## ABSTRACT

**STUDY QUESTION:** Are human ovarian aging and the age-related female fertility decline caused by oxidative stress and mitochondrial dysfunction in oocytes?

**SUMMARY ANSWER:** We found oxidative damage in oocytes of advanced maternal age, even at the primordial follicle stage, and confirmed mitochondrial dysfunction in such oocytes, which likely resulted in the use of alternative energy sources.

**WHAT IS KNOWN ALREADY:** Signs of reactive oxygen species-induced damage and mitochondrial dysfunction have been observed in maturing follicles, and even in early stages of embryogenesis. However, although recent evidence indicates that also primordial follicles have metabolically active mitochondria, it is still often assumed that these follicles avoid oxidative phosphorylation to prevent oxidative damage in dictyate arrested oocytes. Data on the influence of ovarian aging on oocyte metabolism and mitochondrial function are still limited.

**STUDY DESIGN, SIZE, DURATION:** A set of 39 formalin-fixed and paraffin-embedded ovarian tissue biopsies were divided into different age groups and used for immunofluorescence analysis of oxidative phosphorylation activity and oxidative damage to proteins, lipids, and DNA. Additionally, 150 immature oocytes (90 germinal vesicle oocytes and 60 metaphase I oocytes) and 15 cumulus cell samples were divided into different age groups and used for targeted metabolomics and lipidomics analysis.

**PARTICIPANTS/MATERIALS, SETTING, METHODS:** Ovarian tissues used for immunofluorescence microscopy were collected through PALGA, the nationwide network, and registry of histo- and cytopathology in The Netherlands. Comprehensive metabolomics and lipidomics were performed by liquid–liquid extraction and full-scan mass spectrometry, using oocytes and cumulus cells of women undergoing ICSI treatment based on male or tubal factor infertility, or fertility preservation for non-medical reasons.

**MAIN RESULTS AND THE ROLE OF CHANCE:** Immunofluorescence imaging on human ovarian tissue indicated oxidative damage by protein and lipid (per)oxidation already at the primordial follicle stage. Metabolomics and lipidomics analysis of oocytes and cumulus cells in advanced maternal-age groups demonstrated a shift in the glutathione-to-oxigluthathione ratio and depletion of phospholipids. Age-related changes in polar metabolites suggested a decrease in mitochondrial function, as demonstrated by NAD<sup>+</sup>, purine, and pyrimidine depletion, while glycolysis substrates and glutamine accumulated, with age. Oocytes from women of advanced maternal age appeared to use alternative energy sources like glycolysis and the adenosine salvage pathway, and possibly ATP which showed increased production in cumulus cells.

**LIMITATIONS, REASONS FOR CAUTION:** The immature oocytes used in this study were all subjected to ovarian stimulation with high doses of follicle-stimulating hormones, which might have concealed some age-related differences.

**WIDER IMPLICATIONS OF THE FINDINGS:** Further studies on how to improve mitochondrial function, or lower oxidative damage, in oocytes from women of advanced maternal age, for instance by supplementation of NAD<sup>+</sup> precursors to promote mitochondrial

Received: March 9, 2023. Revised: August 16, 2023. Editorial decision: August 25, 2023.

© The Author(s) 2023. Published by Oxford University Press on behalf of European Society of Human Reproduction and Embryology.

This is an Open Access article distributed under the terms of the Creative Commons Attribution-NonCommercial License (<https://creativecommons.org/licenses/by-nc/4.0/>), which permits non-commercial re-use, distribution, and reproduction in any medium, provided the original work is properly cited. For commercial re-use, please contact journals.permissions@oup.com

biogenesis, are warranted. In addition, supplementing the embryo medium of advanced maternal-age embryos with such compounds could be a treatment option worth exploring.

**STUDY FUNDING/COMPETING INTEREST(S):** The study was funded by the Amsterdam UMC. The authors declare to have no competing interests.

**TRIAL REGISTRATION NUMBER:** N/A.

**Keywords:** mitochondrial dysfunction / oxidative damage / ovarian ageing / oocyte quality / NAD<sup>+</sup>

## Introduction

Chances of reproductive success in humans decline with increasing female age, a phenomenon known as ovarian aging (Schieve *et al.*, 2003; Eijkemans *et al.*, 2014; CDC, 2016). Although the age-related decline in female reproductive success appears largely dependent on the age-related decrease in oocyte quality (CDC, 2016), the driving force behind the decrease in oocyte quality with increasing female age is not yet fully understood (Kirkwood, 1998; Chiang *et al.*, 2020; Polonio *et al.*, 2020). One of the suggested mechanisms responsible for ovarian aging is the accumulation of reactive oxygen species (ROS)-induced damage, which has been associated with mitochondrial dysfunction (Hekimi *et al.*, 2011; Wang *et al.*, 2013; May-Panloup *et al.*, 2016; Lefkimmatis *et al.*, 2021). Mitochondrial dysfunction can in turn result in the failure of multiple cell organelles, apoptosis, and cellular senescence (Wang *et al.*, 2013; Vasileiou *et al.*, 2019).

Female meiosis initiates prenatally in the fetal gonads but arrests at the end of the first meiotic prophase just before the first meiotic division would otherwise occur (Faddy *et al.*, 1992). Already before birth, these so-called dictyate arrested oocytes reside in primordial follicles, consisting of the dictyate arrested oocyte and supporting granulosa cells, which are then waiting in the ovary to be stimulated for maturation, a period that can span 40+ years (Faddy *et al.*, 1992). During this period of cell cycle arrest, the primordial follicles maintain basic metabolism to stay alive, while being exposed to environmental factors. Even in a situation where only basic metabolism is needed to maintain cell homeostasis for a long time, cells can get exposed to ROS-induced oxidative damage and mitochondrial dysfunction (Cinco *et al.*, 2016; Ahmed *et al.*, 2019).

During the reproductive years of life in women, under the influence of follicle-stimulating hormone, follicles start to mature in the ovary, a process called folliculogenesis. Folliculogenesis starts at the primordial follicle stage. The primordial follicle consists of a germinal vesicle (GV) oocyte with few surrounding flattened granulosa cells. This is the stage at which follicles reside from birth onward until they are stimulated for maturation (Fig. 1A). During the primary follicle stage, the surrounding granulosa cells increase in number and become more cubically shaped (Fig. 1B). In the secondary follicle stage, the oocyte increases in size and the surrounding granulosa cells form multiple layers (Fig. 1C). During the antral follicle stage, the final stage of folliculogenesis before ovulation, a fluid filled cavity develops between different layers of granulosa cells (Fig. 1D). After ovulation, the oocyte resumes meiosis I, through the metaphase I (MI) stage until it finally reaches the metaphase II stage where it arrests again until fertilization. The granulosa cells still associated with these oocytes are referred to as cumulus cells.

As a potential mechanism to limit ROS-induced damage in primordial follicles, it has been suggested that primordial follicles avoid using oxidative phosphorylation as an energy source and preferably rely on anaerobic glycolysis. However, recent evidence shows that oocytes already display signs of oxidative damage during the earliest stages of folliculogenesis and the

mitochondria are already metabolically active (Jansen and de Boer, 1998; Van Blerkom, 2011; Bradley and Swann, 2019; Wang *et al.*, 2020). During later stages of folliculogenesis, and even early stages of embryogenesis, mitochondria become the primary energy source and play an important role during spindle formation (Wilding *et al.*, 2003; Hashimoto *et al.*, 2017). Signs of ROS-induced damage and mitochondrial dysfunction have been observed during these later stages of folliculogenesis and embryogenesis (Wilding *et al.*, 2001; May-Panloup *et al.*, 2016; Wang *et al.*, 2017; Pasquariello *et al.*, 2019; Wang *et al.*, 2021). We postulate that ROS-induced damage and mitochondrial dysfunction may already occur in primordial follicles and thus play a major role in ovarian aging.

In this study, we investigated the role of declining metabolism in human ovarian aging and found that older oocytes indeed display all the investigated hallmarks associated with oxidative stress and mitochondrial dysfunction.

## Materials and methods

### Ethical approval

The protocol of the study was discussed by the local Medical Ethical Committee and it was decided that the study adhered to national guidelines.

### Experimental model

Ovarian tissue was collected through PALGA: 'the nationwide network and registry of histo- and cytopathology in The Netherlands' (Casparie *et al.*, 2007). We collected ovarian tissue stored in The Netherlands after surgery between 1991 and 2018. Ovarian tissue samples were fixed in 10% formalin, embedded in paraffin, and divided into different age groups: 19–29 (14 follicles), 30–34 (9 follicles), 35–39 (14 follicles), and 40–45 (22 follicles) years. For more details, see [Supplementary Table S1](#). A tissue sample was excluded if the pathology report included malignancies, polycystic ovarian syndrome, or preventive resection due to the woman being BRCA mutation carrier. Further patient characteristics were not provided. Informed consent was received by the Dutch institutions that collected and sent the tissues through PALGA. A total of 39 ovarian tissue samples of individual patients were assessed.

This study also included 150 immature oocytes (90 GV oocytes and 60 MI oocytes) (not suitable for ICSI as they were immature) and 15 cumulus cell samples of women undergoing ICSI treatment based on male or tubal factor infertility, or fertility preservation for non-medical reasons, in the Amsterdam UMC, at the location of the Academic Medical Center. Women were excluded if they, or their partners, were HIV or hepatitis B/C positive. For metabolomics and lipidomics on human oocytes, 10 oocytes per analysis were pooled. Sibling oocytes were kept in the same pool. Each analysis was repeated three times. Women were divided in three age groups: 23–34, 35–37, and 38–42 years of age for GV oocytes, and two age groups for MI oocytes: 23–34 and 35–42 years. The following sample numbers were included in the

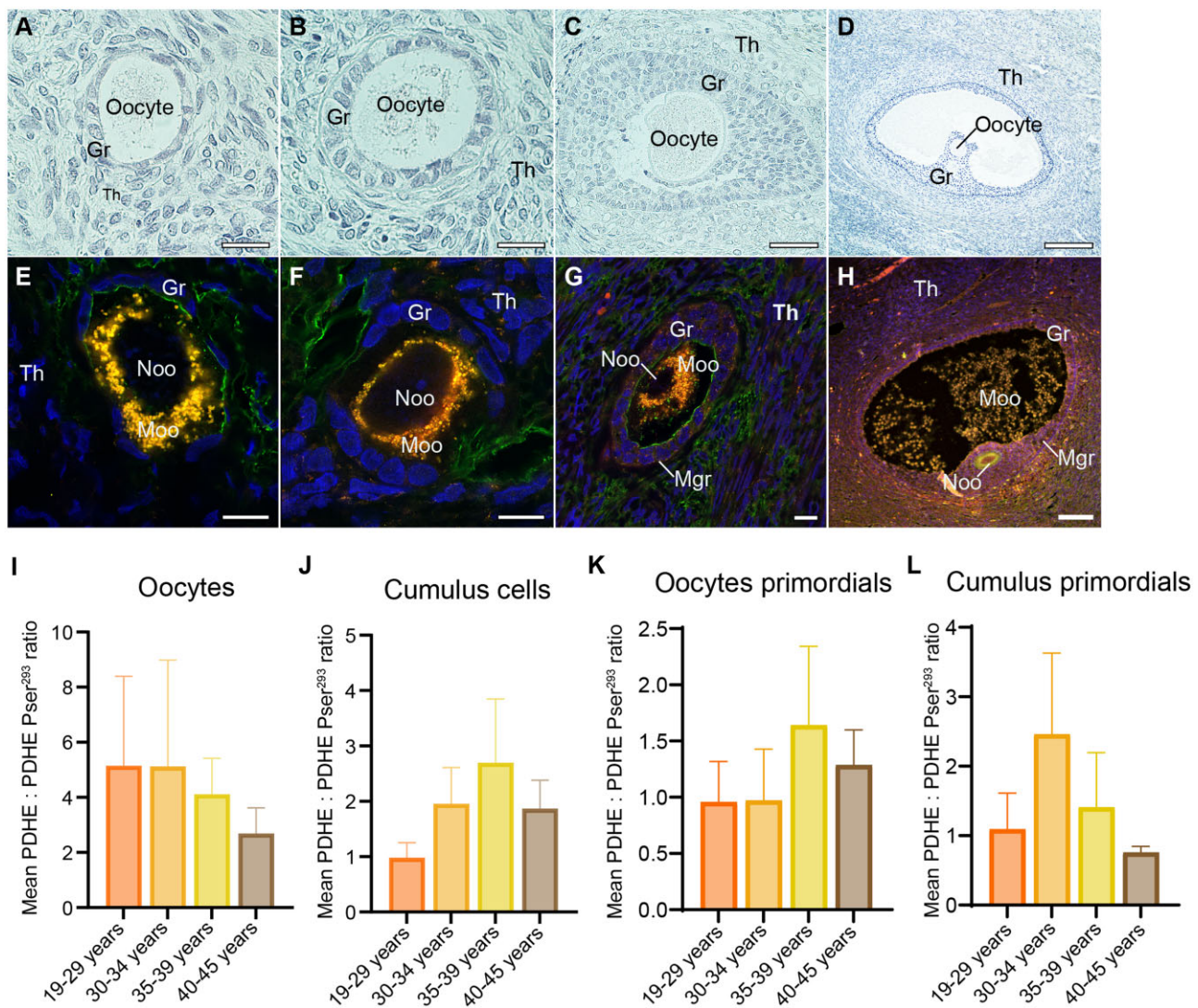


**Figure 1.** Pyruvate dehydrogenase (PDH) activation status in different stages of folliculogenesis of human oocytes. Upper row: staining of different stages of folliculogenesis. Lower row: Immunofluorescence staining of PDHE (pyruvate dehydrogenase E1 component) in different stages of folliculogenesis. (A) Primordial follicle hematoxylin and eosin staining (scale bar 20  $\mu$ m). (B) Primary follicle hematoxylin and eosin staining (scale bar 20  $\mu$ m). (C) Secondary follicle hematoxylin and eosin staining (scale bar 50  $\mu$ m). (D) Antral follicle hematoxylin and eosin staining (scale bar 200  $\mu$ m). (E) Primordial follicle immunofluorescence staining (scale bar 10  $\mu$ m). (F) Primary follicle immunofluorescence staining (scale bar 10  $\mu$ m). (G) Secondary follicle immunofluorescence staining (scale bar 10  $\mu$ m). (H) Antral follicle immunofluorescence staining (scale bar 100  $\mu$ m). (I) Mean ratio of PDHE:PDHE1 $\alpha$  pSer<sup>293</sup> immunofluorescence staining as an indicator of oxidative phosphorylation activity per age group in oocytes. (J) Mean ratio of PDHE:PDHE1 $\alpha$  pSer<sup>293</sup> immunofluorescence staining as an indicator of oxidative phosphorylation activity per age group in cumulus cells. (K) Mean ratio of PDHE:PDHE1 $\alpha$  pSer<sup>293</sup> immunofluorescence staining as an indicator of oxidative phosphorylation activity per age group in oocytes from primordial follicles. (L) Mean ratio of PDHE:PDHE1 $\alpha$  pSer<sup>293</sup> immunofluorescence staining as an indicator of oxidative phosphorylation activity per age group in cumulus (granulosa) cells from primordial follicles. Gr: granulosa/cumulus cells; Th: theca cells. Channels: red: PDHE; yellow: phosphorylated PDH (inactive PDH); blue: DAPI (DNA); green: wheat germ agglutinin (WGA; membrane). Noo: nucleus oocyte; Moo: mitochondria oocyte; Mgr: mitochondria granulosa cells.

study: GV oocytes 23–34 years, 17 women; MI oocytes 23–34 years, 21 women; GV 35–37 years, 16 women; MI oocytes 35–42 years, 24 women; and GV oocytes 38–42 years, 15 women. The following cumulus cell samples were also included: 23–34 years, 5 women; 35–37 years, 5 women; and 38–42 years, 5 women. Cumulus cell samples were not pooled and each analysis was repeated five times.

### Follicle identification using hematoxylin eosin

To determine whether follicles were present in the received tissues, tissues were cut into 5- $\mu$ m-thick sections. For dewaxing and hydration, sections were treated with xylene (VWR chemicals), after which they were exposed to an ethanol gradient. The

sections were rinsed in distilled water for 3 min and stained with hematoxylin (Roth) for 5 min. After staining, the sections were rinsed twice shortly with distilled water for half a minute and placed under running tap water for 10 min. Subsequently, the sections were stained with eosin (VWR chemicals) in 70% ethanol for at least 3 min. The sections were then shortly rinsed, dehydrated using an ethanol-increasing gradient and xylene, and mounted using Entellan (Sigma-Aldrich).

### Immunofluorescence of mitochondria and oxidative phosphorylation use

When at least one follicular stage was identified in an ovarian section, immunofluorescence staining was performed. Again,



tissues were cut into 5- $\mu$ m-thick sections, dewaxed and hydrated, after which they were shortly washed in distilled water. For antigen retrieval, sections were heated in 0.01 M sodium citrate until boiling for 10 min in a microwave and afterwards placed under running tap water for 10 min. All slides were subsequently washed in TBS and incubated with 100  $\mu$ l Superblock (Scytek Laboratories) at room temperature for 1 h, to prevent a-specific binding of antibodies. The slides were incubated overnight at 4°C with primary antibodies or 200  $\mu$ g/ml mouse IgG (Vector Labs) and 200  $\mu$ g/ml rabbit IgG (Vector Labs) for negative controls. Primary antibodies used in this study were 5  $\mu$ g/ml Mouse monoclonal anti-Pyruvate Dehydrogenase E1- $\alpha$  subunit antibody (Abcam) and 10  $\mu$ g/ml Rabbit polyclonal phosphoDetect™ PDHE1 $\alpha$  pSer<sup>293</sup> (PDHA) (Merck). On the second day, the slides were washed three times for 10 min with TBS including 0.1% Tween-20 and incubated with secondary antibodies: 2 mg/ml Abberior STAR fluorescence 635p, Goat anti Mouse (Abberior) and 2 mg/ml Abberior STAR fluorescence 580, Goat anti Rabbit (Abberior) for 1 h. Subsequently, the slides were washed with TBS and incubated with 1 mg/ml 4',6-diamidino-2-phenylindole (DAPI) (Sigma) for 5 min. For cell surface visualization, the fluorescent lectin wheat germ agglutinin (WGA) (Thermo Fisher) was used in a concentration of 1 mg/ml in TBS for 5 min. Lastly, the slides were washed with TBS, embedded with Prolong © Gold Antifade Reagent, and placed at 4°C.

Z-stack images of follicles at different developmental stages were taken on a Leica SP8 fluorescence microscope with stimulated emission depletion. Depending on follicle size, a 100 $\times$  or 40 $\times$  oil immersion lens with a Z-stack step size of 0.15  $\mu$ m with a total of 7 steps was used with Leica Application Suite X. Settings remained unchanged during follicle imaging. All images underwent deconvolution with Huygens Professional version 18.04.

To measure oxidative damage, immunofluorescence was carried out as described above using 2  $\mu$ g/ml Mouse anti-8-Hydroxy-2'-deoxyguanosine (JaICA) visualizing DNA oxidation, 4  $\mu$ g/ml Mouse anti-4-Hydroxynonenal Monoclonal Antibody (Thermo Fisher) visualizing lipid peroxidation, or 10  $\mu$ g/ml Mouse Anti-3-Nitrotyrosine antibody (Abcam) visualizing nitrated proteins. For negative controls, Mouse IgG (Vector Labs) in the same concentration as the antibodies were used. As the secondary antibody, 2  $\mu$ g/ml fluorescence AF555 (Invitrogen) was used. DAPI and WGA were used as counterstaining. All sections were stained at the same time to minimize technical variety. Images were taken on a Leica D5000B Microscope with 40 $\times$  air objective.

Image analysis was done on images after deconvolution using Leica Application Suite X. Mean immunofluorescence intensity of the different channels representing different antibody stainings was measured by drawing a region of interest around the oocyte and surrounding cumulus cells. Immunofluorescence intensity ratios were determined for the PDHE and PDHE1 $\alpha$  pSer<sup>293</sup> antibodies by dividing the immunofluorescence intensity of PDHE by the immunofluorescence intensity of PDHE1 $\alpha$  pSer<sup>293</sup> (PDHE:PDHE1 $\alpha$  pSer<sup>293</sup>) and were calculated and compared between the different stages of folliculogenesis and between the different age groups. IBM SPSS Statistics 25.0 was used for statistical analysis. Differences between developmental stages and age groups were calculated using the Mann-Whitney U-test or Kruskal-Wallis test to compare all age groups and/or developmental stages. Differences were considered significant in case of a P-value of <0.05.

Fluorescence intensity of the different oxidative damage antibodies was measured using Leica Application Suite AF. To minimize technical variety, all sections were stained at the same time

and imaged with the exactly the same microscopy settings. Differences in fluorescence intensity between age groups were calculated using the Mann-Whitney U-test with IBM SPSS Statistics 25.0. Differences were considered significant in case of a P-value of <0.05. Images were deconvolved with Huygens Professional version 22.10 (Scientific Volume Imaging, The Netherlands), using the classic MLE algorithm, with acuity: -5.3 after quantification of the signal.

## Targeted metabolomics and lipidomics on human oocytes and cumulus cells

Metabolomics and lipidomics were performed as previously described, with minor adjustments (Schomakers *et al.*, 2022). For each sample, ~150 000 cumulus cells or exactly 10 oocytes were added to a 2-ml Eppendorf Safe-Lock tube. In the same 2-ml tube, the following internal standards, dissolved in water, were added for metabolomics: adenosine-<sup>15</sup>N<sub>5</sub>-monophosphate (5 nmol), adenosine-<sup>15</sup>N<sub>5</sub>-triphosphate (5 nmol), D<sub>4</sub>-alanine (0.5 nmol), D<sub>7</sub>-arginine (0.5 nmol), D<sub>3</sub>-aspartic acid (0.5 nmol), D<sub>3</sub>-carnitine (0.5 nmol), D<sub>4</sub>-citric acid (0.5 nmol), <sup>13</sup>C<sub>1</sub>-citrulline (0.5 nmol), <sup>13</sup>C<sub>6</sub>-fructose-1,6-diphosphate (1 nmol), <sup>13</sup>C<sub>2</sub>-glycine (5 nmol), guanosine-<sup>15</sup>N<sub>5</sub>-monophosphate (5 nmol), guanosine-<sup>15</sup>N<sub>5</sub>-triphosphate (5 nmol), <sup>13</sup>C<sub>6</sub>-glucose (10 nmol), <sup>13</sup>C<sub>6</sub>-glucose-6-phosphate (1 nmol), D<sub>3</sub>-glutamic acid (0.5 nmol), D<sub>5</sub>-glutamine (0.5 nmol), D<sub>5</sub>-glutathione (1 nmol), <sup>13</sup>C<sub>6</sub>-isoleucine (0.5 nmol), D<sub>3</sub>-lactic acid (1 nmol), D<sub>3</sub>-leucine (0.5 nmol), D<sub>4</sub>-lysine (0.5 nmol), D<sub>3</sub>-methionine (0.5 nmol), D<sub>6</sub>-ornithine (0.5 nmol), D<sub>5</sub>-phenylalanine (0.5 nmol), D<sub>7</sub>-proline (0.5 nmol), <sup>13</sup>C<sub>3</sub>-pyruvate (0.5 nmol), D<sub>3</sub>-serine (0.5 nmol), D<sub>6</sub>-succinic acid (0.5 nmol), D<sub>5</sub>-tryptophan (0.5 nmol), D<sub>4</sub>-tyrosine (0.5 nmol), and D<sub>8</sub>-valine (0.5 nmol). In the same 2-ml tube, the following amounts of internal standards, dissolved in 1:1 (v/v) methanol:chloroform, were added for lipidomics: bis(monoacylglycero)phosphate BMP(14:0)2 (0.2 nmol), ceramide-1-phosphate C1P(d18:1/12:0) (0.125 nmol), D<sub>7</sub>-cholesteryl ester CE(16:0) (2.5 nmol), ceramide Cer(d18:1/12:0) (0.125 nmol), ceramide Cer(d18:1/25:0) (0.125 nmol), cardiolipin CL(14:0)4 (0.1 nmol), diacylglycerol DAG(14:0)2 (0.5 nmol), glucose ceramide GlcCer(d18:1/12:0) (0.125 nmol), lactose ceramide LacCer(d18:1/12:0) (0.125 nmol), lysophosphatidic acid LPA(14:0) (0.1 nmol), lysophosphatidylcholine LPC(14:0) (0.5 nmol), lysophosphatidylethanolamine LPE(14:0) (0.1 nmol), lysophosphatidylglycerol LPG(14:0) (0.02 nmol), phosphatidic acid PA(14:0)2 (0.5 nmol), phosphatidylcholine PC(14:0)2 (2 nmol), phosphatidylethanolamine PE(14:0)2 (0.5 nmol), phosphatidylglycerol PG(14:0)2 (0.1 nmol), phosphatidylinositol PI(8:0)2 (0.5 nmol), phosphatidylserine PS(14:0)2 (5 nmol), sphinganine 1-phosphate S1P(d17:0) (0.125 nmol), sphinganine-1-phosphate S1P(d17:1) (0.125 nmol), ceramide phosphocholines SM(d18:1/12:0) (2.125 nmol), sphingosine SPH(d17:0) (0.125 nmol), sphingosine SPH(d17:1) (0.125 nmol), and triacylglycerol TAG(14:0)2 (0.5 nmol). After adding the internal standards, solvents were added to each sample, for a total of 500  $\mu$ l of water, 500  $\mu$ l of methanol, and 1 ml of chloroform. Samples were then thoroughly mixed, followed by centrifugation for 10 min at 14 000 rpm (20 000g), creating a two-phase system with protein precipitate in the middle.

## Metabolomics

The top layer, containing the polar phase, was transferred to a new 1.5-ml tube and dried using a vacuum concentrator at 60°C. Dried samples were reconstituted in 50  $\mu$ l 6:4 (v/v) methanol:water. Metabolites were analyzed using a Waters Acquity ultra-high performance liquid chromatography system coupled to a Bruker Impact II<sup>TM</sup> Ultra-High Resolution

Qq-Time-Of-Flight mass spectrometer. Samples were kept at 12°C during analysis and 5 µl of each sample was injected. The injection order was randomized, with a pooled QC sample measured at the start, end, and between every 10 samples. Chromatographic separation was achieved using a Merck Millipore SeQuant ZIC-cHILIC column (PEEK 100 mm × 2.1 mm, 3 µm particle size). Column temperature was held at 30°C. Mobile phase consisted of (A) 1:9 (v/v) acetonitrile:water and (B) 9:1 (v/v) acetonitrile:water, both containing 5 mmol/l ammonium acetate. Using a flow rate of 0.25 ml/min, the LC gradient consisted of: 100% B for 0–2 min, reach 0% B at 28 min, 0% B for 28–30 min, reach 100% B at 31 min, 100% B for 31–32 min. Column re-equilibration was achieved by increasing the flow rate to 0.4 ml/min at 100% B for 32–35 min. MS data were acquired using both positive and negative ionization in full-scan mode over the range of *m/z* 50–1200. Data were analyzed using Bruker TASQ software version 2.1.22.3. All reported metabolite intensities were normalized to the number of oocytes for oocyte data, or the total adenosine nucleotide (TAN) pool for cumulus cells, as well as to internal standards with comparable retention times and response in the MS. Metabolite identification has been based on a combination of accurate mass, (relative) retention times and fragmentation spectra, compared to the analysis of a library of standards.

### Lipidomics

The bottom layer of the extraction, containing the apolar phase, was transferred to a glass vial and evaporated under a stream of nitrogen at 60°C. The residue was dissolved in 100 µl of 1:1 (v/v) methanol: chloroform. Lipids were analyzed using a Thermo Scientific Ultimate 3000 binary HPLC coupled to a Q Exactive Plus Orbitrap mass spectrometer. For normal phase separation, 2 µl of each sample was injected onto a Phenomenex® LUNA silica, 250 mm × 2 mm, 5 µm 100 Å. The injection order was randomized, with a pooled QC sample measured at the start and end, and between every ten samples. The column temperature was held at 25°C. The mobile phase consisted of (A) 85:15 (v/v) methanol:water containing 0.0125% formic acid and 3.35 mmol/l ammonia and (B) 97:3 (v/v) chloroform:methanol containing 0.0125% formic acid. Using a flow rate of 0.3 ml/min, the LC gradient consisted of: 10% A for 0–1 min, reaching 20% A at 4 min, reaching 85% A at 12 min, reaching 100% A at 12.1 min, 100% A for 12.1–14 min, reaching 10% A at 14.1 min, 10% A for 14.1–15 min. For reversed phase separation, 5 µl of each sample was injected onto a Waters HSS T3 column (150 mm × 2.1 mm, 1.8-µm particle size). Column temperature was held at 60°C. The mobile phase consisted of (A) 4:6 (v/v) methanol:water and B 1:9 (v/v) methanol:isopropanol, both containing 0.1% formic acid and 10 mmol/l ammonia. Using a flow rate of 0.4 ml/min, the LC gradient consisted of: 100% A at 0 min, reaching 80% A at 1 min, reaching 0% A at 16 min, 0% A for 16–20 min, reaching 100% A at 20.1 min, 100% A for 20.1–21 min. MS data were acquired using negative and positive ionization using continuous scanning over the range of *m/z* 150 to *m/z* 2000. Data were analyzed using a lipidomics pipeline developed in-house, written in the R programming language (<http://www.r-project.org>). All reported lipids were normalized to corresponding internal standards according to lipid class, as well as to the number of oocytes for oocyte data, or the TAN pool for cumulus cells. Lipid identification has been based on a combination of accurate mass, (relative) retention times, and the injection of relevant standards.

### Data analysis

All data generated with metabolomics and lipidomics can be found in [Supplementary Tables S2, S3, S4, and S5](#). For the metabolomics, a partial least square regression discriminant analysis (PLS-DA) was used to discriminate between the different age groups using the programming language R and the mixOmics package. Differential changes of metabolites and lipids contributing to the discrimination between the different age groups, were determined according to the Variable Importance in Projection (VIP) score extracted from the PLS-DA. Since different age groups showed a distinct pattern in the PLS-DA of different age groups for the MI and GV oocytes, metabolites with a VIP score of >1 were considered significant. Since the PLS-DA of cumulus cells could not distinguish different age groups, differences were calculated using one-way ANOVA, with a significance cut-off of <0.05. PLS-DA was also able to clearly distinct age groups in MI and GV oocytes. Age-related changes for individual lipids can be found in the [Supplementary Table S2](#). To investigate age-related changes in lipid classes rather than individual lipids, *P*-values were calculated by a Student's *t*-test, one-way ANOVA or Kruskal–Wallis test, depending on normality of distribution. A *P*-value of <0.05 was considered significant.

## Results

### All follicular stages, including primordial follicles, display mitochondrial activity

To investigate possible age-related changes in human follicles, we collected formalin-fixed paraffin-embedded ovarian tissue samples of 39 women of different ages who underwent surgery for non-malignant purposes. In hematoxylin and eosin-stained tissue-sections, the presence of primordial, primary, secondary, and antral follicles was assessed ([Fig. 1A–D](#)). If at least one follicular stage was present in a tissue section, the tissue was used for further super resolution immunofluorescence microscopy.

Since oxidative stress and mitochondrial dysfunction have often been implicated in matured oocytes of advanced maternal age ([May-Panloup et al., 2016; Kasapoğlu and Seli, 2020](#)), we decided to study the activation status of the mitochondrial gatekeeper enzyme pyruvate dehydrogenase (PDH) during all different stages of folliculogenesis. PDH is a major regulator of glucose metabolism, directing pyruvate to oxidative phosphorylation, rather than to anaerobic glycolysis. To this end, we used antibodies against the PDH subunit pyruvate dehydrogenase E1- $\alpha$  (PDHE1 $\alpha$ ), representing the total amount of PDH, in combination with antibodies against phosphorylated PDHE1 $\alpha$  (PDHE1 $\alpha$  pSer<sup>293</sup>), representing its inactive state. The active proportion of PDH was calculated by measurement and quantification of the PDHE1 $\alpha$  to PDHE1 $\alpha$  pSer<sup>293</sup> fluorescent signal intensity ratios. The PDHE1 $\alpha$  pSer<sup>293</sup> staining, represented in yellow in [Fig. 1E–H](#), co-localized with the PDHE1 $\alpha$  antibody, which is represented in red. To define the border between the oocyte and surrounding granulosa cells, we used the membrane marker WGA (represented in green) and DAPI (represented in blue) to stain DNA ([Fig. 1E–H](#)). Since the oocyte nucleus is very large in size, the DAPI staining more strongly visualizes the surrounding granulosa and theca cells. The PDH activation status, i.e. PDHE1 $\alpha$  to PDHE1 $\alpha$  pSer<sup>293</sup> ratio, was calculated for all stages of folliculogenesis. We next compared how the PDH activation status changed in oocytes and granulosa cells with increasing female age. We included the following number of follicles, at several follicular stages, into the analysis of the different age groups: 19–29 years, 14 follicles; 30–34 years, 9 follicles; 35–39 years, 14 follicles, and 40–45 years,

22 follicles (Supplementary Table S1). Although there was a trend toward a lower ratio and hence lower PDH activation status, when all follicles were analyzed, no significant age-related change in PDH activation status was found in oocytes ( $P=0.612$ ; Fig. 1I) or granulosa/cumulus cells ( $P=0.334$ ; Fig. 1J) in regard to PDH activation status. Also, between the different follicle stages, no significant differences in PDH activation status could be observed (oocytes  $P=0.1801$ , granulosa cells  $P=0.4094$ ). Unfortunately, the number of tertiary follicles that could be included was too low for such an analysis. However, because ovarian aging occurs predominately at the primordial follicle stage, we additionally analyzed oocytes ( $n=24$ ) and granulosa cells ( $n=24$ ) of this stage. At this follicular stage also, no significant age-related changes were observed in oocytes ( $P=0.876$ , Fig. 1K) or granulosa cells ( $P=0.859$ , Fig. 1L). Negative controls showed no staining for PDHE1 $\alpha$  and PDHE1 $\alpha$  pSer<sup>293</sup> (Supplementary Fig. S1A). Since no difference in PDH activation status throughout folliculogenesis was observed, we hypothesized that ROS-induced cellular damage could potentially already start to accumulate from the earliest stages of folliculogenesis in dictyate arrested oocytes residing in primordial follicles.

### Increased ROS-induced protein and lipid damage in primordial follicles of advanced maternal age

Since ROS can already be created during the primordial follicle stage, we further investigated whether ROS-induced damage was already detectable at the primordial follicle stage and thus could contribute to ovarian aging. For this, we visualized ROS-induced damage at the protein, lipid and DNA level (Lim and Luderer, 2011). To identify a possible age-dependent trend in ROS-induced damage, a linear regression analysis was carried out for the maximum intensity of the different antibodies and female age. Protein oxidation was visualized using antibodies against 3-nitrotyrosine (NTY) (Fig. 2A), and was significantly increased in oocytes with increasing female age (Fig. 2B). The same was true for lipid peroxidation, which was visualized using antibodies against 4-hydroxynonenal (4HNE) (Fig. 2C and D). In contrast, DNA oxidation, visualized using an antibody against 8-Oxo-2'-deoxyguanosine (8OHdG) (Fig. 2E), did not differ between different female ages (Fig. 2F). Negative controls showed no staining for ROS-induced antibodies (Supplementary Fig. S1B–D). Together, these data indicated the accumulation of oxidative damage to proteins and lipids in oocytes of advanced maternal age already at the primordial follicle stage.

### Targeted metabolomics and lipidomics suggest impaired mitochondrial function in oocytes of advanced maternal age

Since we found higher ROS-induced damage to lipids and proteins in aged primordial follicles, we questioned whether cellular metabolism could be impaired in aged oocytes. Therefore, we performed metabolomics and lipidomics by UPLC–mass spectrometry on GV oocytes, MI oocytes and cumulus cells associated with these oocytes. The oocytes were collected after ovarian stimulation for ICSI treatment or oocyte preservation treatment but appeared to be immature so could not be used for treatment. To achieve sufficient yield for subsequent metabolomics and lipidomics, 10 oocytes were grouped by age per analysis. Because one ICSI treatment yielded sufficient amounts of cumulus cells, cumulus cell samples did not need to be pooled. Age categories were chosen based on the oocyte quality decline observed with ovarian aging (Schieve et al., 2003) and, for GV oocytes, were

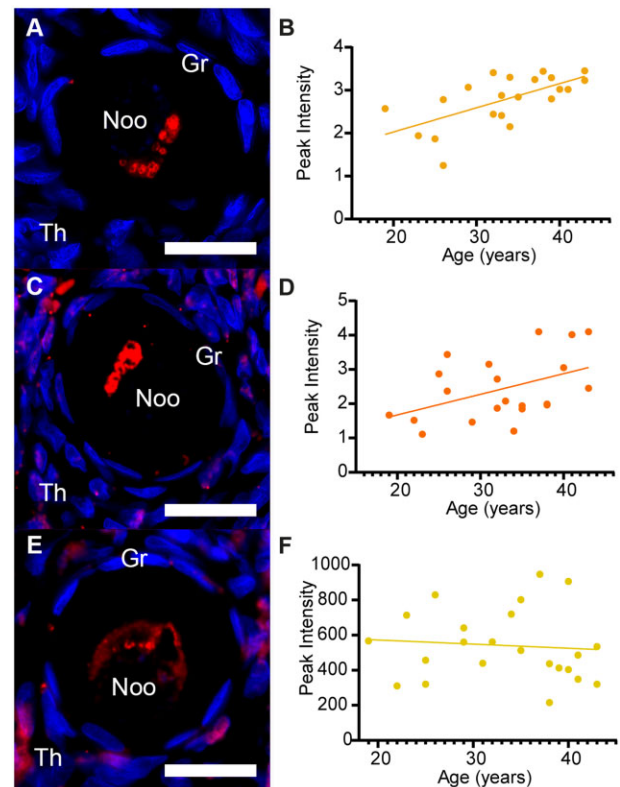


**Figure 2. Reactive oxygen species (ROS) induced damage to proteins and lipids increases with age in primordial follicles.** Immunofluorescence staining of different ROS damage markers in primordial follicles in human ovarian tissue and the simple linear regressions of the peak intensity of these markers with age in human oocytes. (A and B) ROS-induced protein oxidation staining (mouse anti 3-nitrotyrosine) significantly increased with increasing female age,  $R^2 = 0.4092$ ,  $P = 0.002$ . (C and D) ROS-induced lipid peroxidation-staining (mouse anti 4-hydroxynonenal) significantly increased with increasing female age,  $R^2 = 0.2052$ ,  $P = 0.0392$ . (E and F) ROS-induced DNA damage-staining (anti 8-Oxo-2'-deoxyguanosine) did not change with increasing female age,  $R^2 = 0.0073$ ,  $P = 0.6983$ . Scale bars = 20  $\mu$ m. Noo: nucleus oocyte; Gr: granulosa cells; Th: theca cells. Blue: DAPI, red: ROS-induced damage.

characterized as follows: (i) donor age: 23–34 years old, representing good quality oocytes; (ii) donor age: 35–37 years old, oocytes with a gradual decline in quality; (iii) donor age: 38–42 years old, reflecting rapid decline in oocyte quality. MI oocytes were categorized in two age groups, as follows: (i) 23–34 years old and (ii) 35–42 years old. All oocytes were studied in triplicate per category; thus, 30 oocytes were included per category, 150 in total.

Using metabolomics and lipidomics, we detected and annotated 89 polar metabolites and over 1100 lipid species. The metabolome (Fig. 3A and B) and lipidome (Supplementary Fig. S2A and B) of human GV and MI oocytes showed a distinct pattern with increasing female age as identified by PLS-DA (Fig. 3A and B). From this PLS-DA, metabolites with a 'variable of importance in projection' (VIP) score  $>1$  are considered significant and are shown in Fig. 3D for MI oocytes. We performed the same statistical analysis to compare the youngest to the oldest age groups of GV oocytes (Supplementary Fig. S3). For lipidome analysis, we quantified changes of lipid classes; i.e. the sum of lipids belonging to one class, rather than individual lipids, using one-way ANOVA, Student's t-test or a Kruskal–Wallis test ( $P$ -value of  $<0.05$  was considered significant).



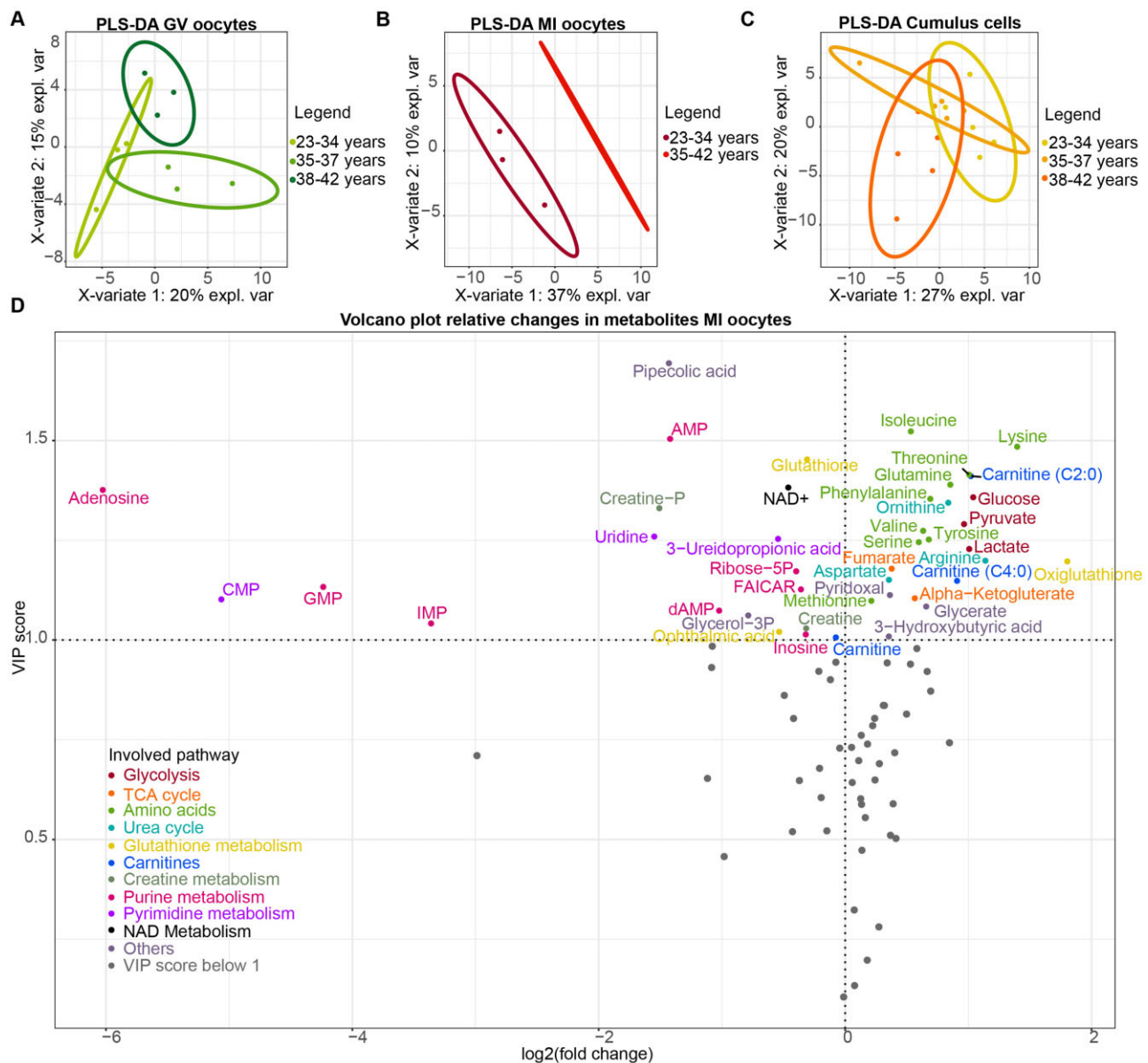


**Figure 3. Age-related metabolite changes in MI and GV oocytes.** (A) PLS-DA (partial least square regression discriminant analysis) analysis of the metabolome of pooled human GV (germinal vesicle) oocytes distinguishes between different female age categories: 23–34, 35–37, and 38–42 years. (B) PLS-DA of the metabolome of pooled human MI (metaphase I) oocytes distinguishes between different female age categories: 23–34 and 35–42 years. (C) PLS-DA of the metabolome of single cumulus cell samples per female age category: 23–34, 35–37, and 38–42 years. There was no clear distinction between different age categories. (D) Volcano plot of relative changes in metabolites of MI oocytes between different age categories based on VIP scores >1, colored by pathway in which they play the most important role.

In cumulus cells, PLS-DA of both the metabolome and lipidome could not distinguish different age groups (Fig. 3C and Supplementary Fig. S2C).

### Increased signs of oxidative stress in aging GV and MI oocytes

Since we found an age-related increase in ROS-induced damage in primordial follicles, we investigated several indicators for oxidative stress through metabolomics in GV and MI oocytes. One of these indicators is the glutathione-to-oxigluthathione ratio (GSH/GSSG) within a cell. In GV oocytes, glutathione did not change with age and oxigluthathione decreased (Fig. 4A and B). In contrast to GV, a decrease in glutathione abundance was observed for older MI oocytes, which was accompanied with an apparent increase of oxigluthathione (Fig. 4A and B). This indicates

a shift toward GSSG and thus increased oxidative stress in MI oocytes of advanced maternal age.

Another indicator for oxidative damage is lipid peroxidation. Lipid peroxidation was already visualized in primordial follicles of women of older ovarian age (Fig. 2B). Using lipidomics, we investigated age-related changes in different lipid classes in GV and MI oocytes. To our surprise, all phospholipids decreased in abundance with increasing age in both GV and MI oocytes (Fig. 4C–I). In GV oocytes, a significant age-related decrease was observed in total phosphatidylserine (PS) and a decreasing trend was seen for phosphatidylcholine (PC), phosphatidylethanolamine (PE), phosphatidylglycerols (PG), and, to lesser extent, phosphatidylinositols (PI) (Fig. 4C–I). In MI oocytes, we found a decreasing trend for PE, PC, PG, and PI (Fig. 4C–I). In addition to lipid classes, many individual lipids changed with increasing female age.

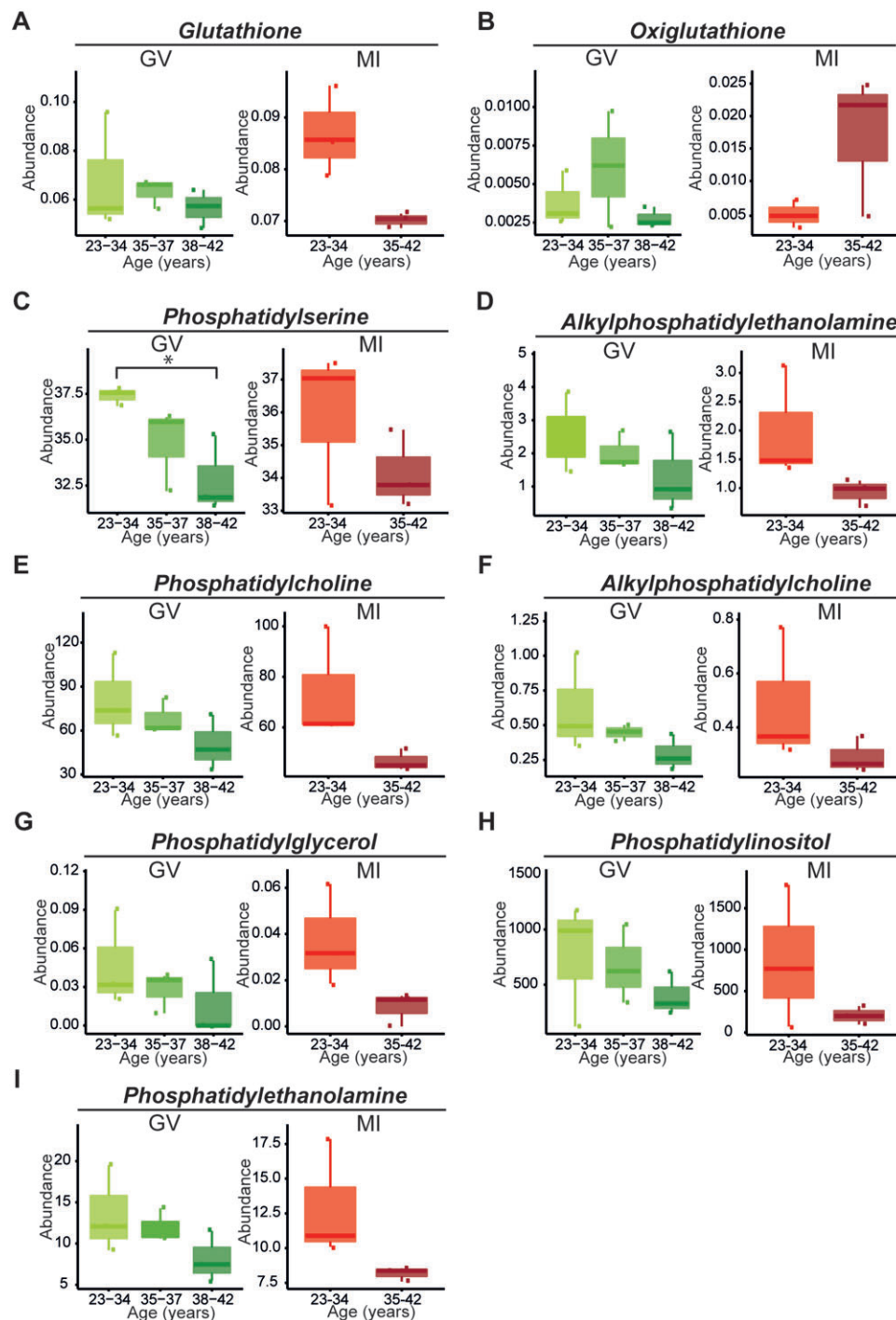


**Figure 4.** Different signs of oxidative stress are seen in GV (germlinal vesicle) and MI (metaphase I) oocytes. (A and B) Glutathione is depleted in aging oocytes during MI, while oxiglutathione accumulates, indicating an increase in oxidative stress. (C and D) Phosphatidylserine significantly decreased with age in GV oocytes and showed a decreasing trend in MI oocytes. Alkylphosphatidylethanolamine showed a decreasing trend with age in GV and MI oocytes. (E–I) Phosphatidylcholine, alkylphosphatidylcholine, phosphatidylglycerol, phosphatidylinositol, and phosphatidylethanolamine show a decreasing trend with age, both in GV and MI oocytes. GV: GV oocytes; MI: MI oocytes.

Supplementary Fig. S4 shows an overview of different individual lipid changes with female age in MI oocytes and all data on individual lipid changes can be found in Supplementary Table S2.

### Metabolites feeding into the TCA cycle accumulate with increasing age in both GV and MI oocytes

The TCA cycle, located in the mitochondria, is mostly known as, but is not limited to, the most important supplier of adenosine

triphosphate (ATP) (Akram, 2014). In both GV and MI oocytes, metabolites associated with glycolysis increased. In GV oocytes, glucose and pyruvate increased with increasing female age (Fig. 5A and B). In MI oocytes, glucose, glucose-6-phosphate (not shown), phosphoenolpyruvate (not shown), pyruvate, and lactate, all showed an increase in oocytes of advanced maternal age, with glucose and pyruvate roughly doubled (Fig. 5A–C). In contrast, metabolites involved in glycolysis did not change with age in cumulus cell samples (Supplementary Table S3).



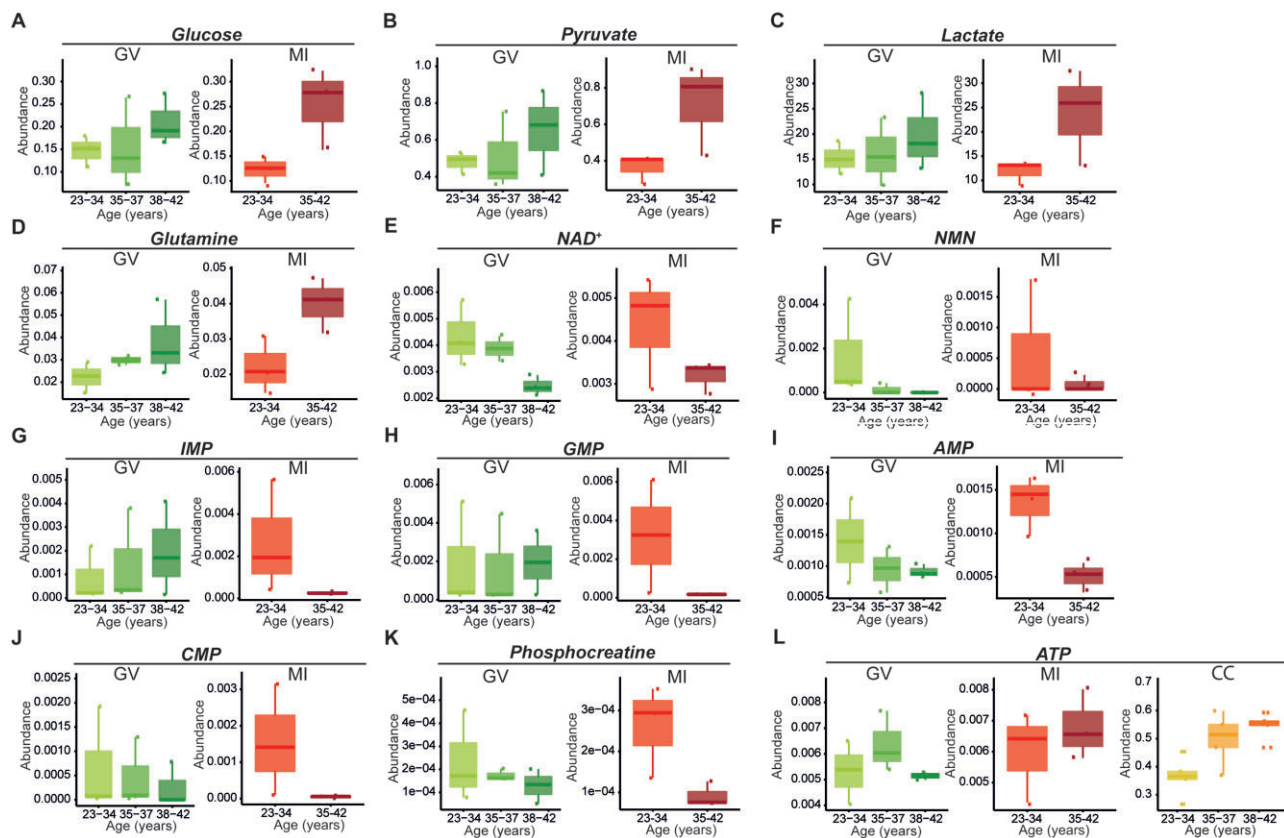


**Figure 5.** Metabolites associated with mitochondrial function are disturbed in aging oocytes, especially in MI oocytes. (A–D) Metabolites that fuel mitochondrial metabolism accumulate with age: glucose, pyruvate, lactate and glutamine. (E and F) Metabolites associated with energy status of the cell diminish in aging oocyte: NAD<sup>+</sup> (nicotinamide adenine dinucleotide) and NMN (nicotinamide mononucleotide). (G–I) Monophosphate nucleotide intermediates that are dependent on mitochondrial metabolism show depletion with age: inosine monophosphate (IMP), guanosine monophosphate (GMP), adenosine monophosphate (AMP), and cytidine monophosphate (CMP) in MI oocytes. (K) Phosphocreatine, together with AMP, is associated with the adenosine salvage pathway, an alternative path to creating ATP, and both were reduced with age. (L) ATP increases in cumulus cells with age, possibly in an attempt to compensate for mitochondrial dysfunction in the aging oocyte. GV: germinal vesicle oocytes; MI: metaphase I oocytes; CC: cumulus cells.

In addition to pyruvate, glutamine functions as mitochondrial fuel. Glutamine also accumulated with age in both GV and MI oocytes (Fig. 5D). TCA cycle intermediates, such as  $\alpha$ -ketoglutarate, succinate, and fumarate, did not change with age in MI oocytes (Supplementary Table S4), while the TCA cycle intermediates succinate and fumarate were decreased in GV oocytes (Supplementary Fig. S4). The fact that substrates feeding into the TCA cycle accumulate with age, while TCA cycle intermediates did not change in MI oocytes, might be indicative of the TCA cycle not being able to process available substrates.

### Impaired nicotinamide adenine dinucleotide (NAD<sup>+</sup>) biosynthesis in older GV and MI oocytes

NAD<sup>+</sup> plays an important role in energy metabolism (Houtkooper et al., 2010; Katsyuba et al., 2020; Zapata-Pérez et al., 2021) and stimulates mitochondrial biogenesis through SIRT1 (Brenmoehl and Hoeflich, 2013). In GV oocytes, we observed a decrease in NAD<sup>+</sup> and nicotinamide mononucleotide (NMN, an NAD<sup>+</sup> precursor) abundance (Fig. 5E and F), while other NAD<sup>+</sup> precursors, kynurenine and nicotinamide riboside (NR), increased with age (Supplementary Fig. S3). The downstream product of kynurenine, quinolinic acid, did not accumulate in GV oocytes (Supplementary Table S5). In MI oocytes, NAD<sup>+</sup> also decreased in abundance with age, but the precursors NMN, kynurenine, and NR all remained unchanged throughout the different age categories (Fig. 5E and F and Supplementary Table S4). Interestingly, NR

was higher with age in cumulus cells (Supplementary Table S3). An age-related decrease in NAD<sup>+</sup> in both GV and MI oocytes could indicate that NAD<sup>+</sup> biosynthesis is impaired in oocytes of women of advanced maternal age. This is specifically true in GV oocytes, since several NAD<sup>+</sup> precursors accumulated with age but do not result in an increase in NAD<sup>+</sup>.

### Changes in mitochondrial purine and pyrimidine nucleotide biosynthesis in older MI oocytes

Purine and pyrimidine nucleotide biosynthesis is largely carried out by mitochondria and provides the cell with nucleotides (Wang, 2016). The purine nucleotide synthesis pathway requires a significant amount of molecular fuel. For each molecule of inosine monophosphate (IMP) that is generated, five molecules of ATP are required, as well as glutamine, glycine, aspartate, formate and carbon dioxide (Chan et al., 2018). Many of these substrates are produced directly by the mitochondria and it has recently been shown that a large proportion of the purinosomes are grouped together and co-localize with mitochondria (Chan et al., 2018; Yin et al., 2018). In GV oocytes, glycine, and its precursor serine, increased with age (Supplementary Table S5). In MI oocytes, glycine abundance did not change with age, but the precursor serine showed a 1.5-fold increase (Supplementary Table S4). As mentioned above, the glutamine concentration accumulated with age in both GV and MI oocytes (Fig. 5D). Aspartate accumulated in both GV and MI oocytes (Supplementary Tables S4

and S5). The direct precursor to the *de novo* purine synthesis pathway, ribose-5P, is produced in the cytosol and did not show an age-dependent trend in GV oocytes and was decreased in MI oocytes of advanced maternal age. Dramatic differences were observed in the monophosphate end products at the core of this pathway; an almost 10-fold decrease in IMP, a 20-fold decrease in guanosine monophosphate (GMP), and a 2.7-fold decrease in adenosine monophosphate (AMP) were observed in MI oocytes of advanced maternal age (Fig. 4G–I). In GV oocytes, AMP also decreased with increasing age, but IMP increased and GMP did not change with female age (Supplementary Table S5). Decreases were also seen in MI oocytes for 5-formamidoimidazole-4-carboxamide ribotide (FAICAR), inosine and adenosine (Supplementary Table S4). This was not the case for GV oocytes, in which adenosine also decreased, but inosine increased and FAICAR did not change in women of advanced maternal age (Supplementary Table S5). In cumulus cells, metabolites of the purine nucleotide biosynthesis were not affected with age (Supplementary Table S3).

In line with observations in purine metabolism, monophosphate end products of pyrimidine synthesis were also affected strongly in older MI oocytes. Older MI oocytes showed a 33-fold lower abundance in cytidine monophosphate (CMP), a 1.5-fold decrease for the uracil breakdown product 3-ureidopropionic acid, and a 3-fold lower abundance of uridine (Fig. 5J and Supplementary Table S4). In GV oocytes and cumulus cells, no age-dependent changes were observed in pyrimidine synthesis (Supplementary Tables S3 and S5). Together, these results show that the mitochondrial contribution to purine and pyrimidine nucleotide biosynthesis appears highly disrupted with age in MI oocytes.

### Alternative energy sources in aged GV and MI oocytes

As mentioned above, glycolysis intermediates seemed to be increased in GV and MI oocytes of women of advanced maternal age (Fig. 5A–C). Besides increasing glycolysis, oocytes are able to use the adenosine salvage pathway as another alternative energy source to the TCA cycle, for which they use phosphocreatine and AMP (Scantland et al., 2014). AMP was decreased in GV oocytes and in MI oocytes of advanced maternal age (Fig. 5I). GV oocytes and cumulus cells did not show a decrease in phosphocreatine, but in MI oocytes phosphocreatine showed a 2.7-fold decrease (Fig. 5K and Supplementary Table S4). Creatine was also decreased with age in MI oocytes (not in GV oocytes), but only by 1.2-fold (Supplementary Table S4).

It has been previously described that oocytes are supplied with ATP by surrounding cumulus cells through gap junctions (Van Blerkom et al., 2008; Dalton et al., 2014). Therefore, cumulus cells might partly compensate for the loss of ATP due to mitochondrial dysfunction (Kansaku et al., 2017). We observed an increase in ATP levels of cumulus cells with age, while the ATP levels of GV and MI oocytes seemed unchanged (Fig. 5L).

## Discussion

It is often assumed that mitochondria in dictyate arrested oocytes in primordial follicles are largely inactive to prevent ROS-induced oxidative stress. However, increasing evidence indicates that mitochondria in dictyate arrested oocytes are already metabolically active (Van Blerkom, 2011; Bradley and Swann, 2019). Recently, Wang et al. (2020) studied the transcriptomic landscape of ovarian cell types of cynomolgus monkeys during different

stages of folliculogenesis and found that already during early stages of folliculogenesis, antioxidant proteins were downregulated, while oxidative stress markers were upregulated in oocytes of older monkeys (Wang et al., 2020). Using high-resolution fluorescence microscopy, we studied the activation status of the mitochondrial gatekeeper enzyme PDH on human ovarian biopsies of women of different ages and found that mitochondria are indeed active in human dictyate arrested oocytes. In addition, by using immunofluorescence markers, we have shown an age-related increase in lipid peroxidation and protein oxidation, which are clear signs of oxidative damage, in these cells. However, we did not observe an age-related increase in DNA oxidation. Oocytes with excessive DNA damage may have disappeared from the ovarian reserve and were thus not observed. Alternatively, additional oxidative damage caused by formalin fixation material may have masked differences between the age groups. Signs of oxidative damage were also observed in metabolomic and lipidomic analysis of human GV and MI oocytes, which were leftover oocytes from ICSI and oocyte preservation treatments. In aged MI oocytes we found a disturbed glutathione-to-oxogluthathione ratio, and in both MI and GV oocytes, we found a major drop in phospholipids, as will be discussed further below. Besides signs of oxidative stress, we also observed age-related changes that indicate mitochondrial dysfunction: impaired  $\text{NAD}^+$ , purine and pyrimidine pathways, and the use of alternative energy sources such as the adenosine salvage pathway, and increased ATP in surrounding cumulus cells.

We found several metabolic changes that all pointed toward mitochondrial dysfunction in MI and, to lesser extent, GV oocytes of advanced maternal age. The PLS-DA used to analyze the metabolomics dataset could potentially lead to misleading results when relying on a single metabolites (Gromski et al., 2015). However, we use our 'omics' data to explain understandable, and known, metabolic processes which, taken together, all point toward this conclusion. GV oocytes are transcriptionally active, but during their development to metaphase II oocytes, they become transcriptionally silent, which means that they cannot replace degrading gene transcripts anymore (Bouniol-Baly et al., 1999; Ntostis et al., 2021). Therefore, age-induced damage is expected to have a more pronounced effect on MI oocytes compared to GV oocytes (Llonch et al., 2021). An increase in glycolytic metabolites in women of older age could point toward an affected TCA cycle but could also point toward an increase in anaerobic glycolysis. Since both pyruvate and glutamine are increased as well, it is more likely that the TCA cycle is unable to process the provided metabolites. The observed impaired  $\text{NAD}^+$  biosynthesis may for example be due to a lack of nucleotides in older oocytes or may point toward a broader dysfunction in the mitochondria (Imai and Guarente, 2014). Besides, a decrease in  $\text{NAD}^+$  can lead to decreased mitochondrial biogenesis, inducing a downward spiral (Katsyuba et al., 2020). MI oocytes of advanced maternal age also showed large decreases in mitochondria-derived substrates and end products, e.g. IMP, GMP, and CMP, of the purine and pyrimidine nucleotide biosynthesis. Since we observed an age-related increase in metabolites related to glycolysis, a decrease in the metabolites of the adenosine salvage pathway, and an increase in ATP content of surrounding cumulus cells, we hypothesize that these sources could be used as alternative energy sources in oocytes of advanced maternal age. Besides this, the changes with age in the GSH/GSSG ratio in MI and GV oocytes, point toward an increased state of oxidative stress in oocytes of advanced maternal age (Zitka et al., 2012). Glutathione itself is involved in numerous oocyte and embryo functions. For example, by protecting the

meiotic spindle against oxidative stress, but also by stimulating sperm decondensation required for the development of the male pronucleus after fertilization (Yoshida et al., 1993; Zuelke et al., 1997; Sutovsky and Schatten, 1997; Luberd, 2005). Depletion of the glutathione pool is therefore expected to have adverse effects on the oocyte. Moreover, almost all phospholipid classes in older oocytes in both the GV and MI stage showed a decreasing trend with age. It should be noted that this effect does not necessarily mean an absolute reduction in the total abundance of each class. It seems plausible that products of these affected phospholipids, for example oxidized phospholipids, are not detected using the current method, either because they fall below detection limits or are turned into products that are not annotated. Using an immunofluorescence antibody against 4-hydroxynonenal (another form of lipid peroxidation), we have already found that oocytes of ovarian biopsies of women of advanced maternal age suffer more lipid peroxidation. Oxidation of the phospholipids of advanced maternal-age oocytes also seems in line with the extremely disturbed GSH:GSSG ratio. Phospholipids contain a relatively large number of polyunsaturated fatty acids (PUFAs). PUFAs are more sensitive to this type of destruction than saturated classes, as radicals specifically attack double bonds (Catalá, 2009; Hu et al., 2017). In line with this, de la Barca et al. (2017) found decreased polyunsaturated choline plasmalogens in follicular fluid of women with diminished ovarian reserve, which they also explain by an increase in oxidative stress (de la Barca et al., 2017). Previous studies into aging and oxidative stress in mouse oocytes showed the vulnerability of phospholipids to lipid peroxidation, already at the GV stage of development (Mok et al., 2016). Besides having a function as signaling molecules, phospholipids are found mostly on the cell membrane (Shimada and Terada, 2001; Catalá, 2009), where they are responsible for the structure, and thereby permeability, of the membrane. Therefore, the lower amount of phospholipids may by itself already have a detrimental effect on oocyte function, for example by decreasing the chance of successful fertilization in women of advanced maternal age.

While some research already has been published on the use of metabolomics and lipidomics in reproductive medicine, this concerned non-invasive measurements that were done on culture medium or follicular fluid (de la Barca et al., 2017; Siristatidis et al., 2018; Montani et al., 2019; Bouet et al., 2020; Luti et al., 2020). Although interesting from a clinical perspective, these studies could not unravel the biological mechanisms that play a role in oocyte quality or ovarian aging, since these studies did not measure metabolites in oocytes or cumulus cells. Additionally, previous lipidomic studies were limited in scope, focusing on a small selection of lipids using e.g. MALDI or MRM (Cataldi et al., 2013; Zhang et al., 2020), rather than performing full-scan LC-MS analysis of complex lipids as we have done here, which provides a much more comprehensive picture of the oocyte and cumulus cell lipidomes.

Mechanisms that could improve mitochondrial function in oocytes are interesting to investigate in future studies that aim to solve ovarian aging. Mitochondrial replacement therapy by ooplasm transfer could be a potential treatment for advanced maternal age. However, ooplasm transfer includes medical risks and ethical objections and is therefore not yet a good treatment option for advanced maternal age (Yamada et al., 2021). Other possible treatment options include enhancing the depleted NAD<sup>+</sup> pool or correcting glutathione deficiency in oocytes of advanced maternal age. NAD<sup>+</sup> promotes mitochondrial biogenesis (Brenmoehl and Hoeflich, 2013). In mice, NMN, an NAD precursor

that can boost NAD<sup>+</sup>, has already been shown to improve oocyte quality (Bertoldo et al., 2020), and recently, a pilot clinical trial was published in which glycine and N-acetylcysteine were shown to improve glutathione deficiency and mitochondrial function (Kumar et al., 2021). Therefore, supplementing embryo medium of advanced maternal-age embryos with these compounds could be a treatment option worth exploring.

To achieve sufficient yield for the metabolomics and lipidomics of oocytes, ten oocytes were pooled per analysis. Due to the limited amounts of oocytes available, only three replicates per age group were possible. Therefore, most results did not reach statistical significance, based on a P-value of <0.05 and after correction for multiple testing. Still, the total amount of oocytes included in this study is 150, which is much larger than the number of oocytes used for most human studies so far (Llonch et al., 2021; Trebichalská et al., 2021; Yuan et al., 2021) and, combined with the 39 human ovarian biopsies, this represents a unique dataset.

Ideally, we would have additionally included metaphase II oocytes in our study, but these oocytes are all intended for use in ICSI treatments. GV and MI oocytes are also collected during oocyte retrieval but, due to immaturity, cannot be used for ICSI treatment and could therefore be used in our study. It is important to note that results might have been different if metaphase II oocytes, and especially if naturally ovulated oocytes, had been included. The fact that oocytes used in the current study were all subjected to ovarian stimulation with high doses of follicle-stimulating hormones might also have concealed some age-related differences.

## Supplementary data

Supplementary data are available at *Human Reproduction* online.

## Data availability

The published article includes all metabolomics and lipidomics datasets on GV, MI, and cumulus cell samples generated or analyzed during this study. The data underlying this article are available in the article and in its online [supplementary material](#).

## Acknowledgements

The authors acknowledge the Center for Reproductive Medicine Fertility Laboratory for providing the GV and MI oocytes and cumulus cells for research; PALGA: Dutch Pathology Registry for using human ovarian biopsies (Casparie et al., 2007); Milou Kleijn and Stella Dorrestein for their help optimizing the immunofluorescence assays; Cindy Korver and Saskia van Daalen for running the immunofluorescence assays for ROS-induced damage; Wendy Noort for her help with deconvolution microscopy; Ronald Wanders for critically reading the manuscript; and the Amsterdam Reproduction & Development research institute for financial support (grant number V.000296).

## Authors' roles

M.A.J.S., B.V.S., M.v.W., R.C.I.W., S.M., M.G., R.H.H., and G.H. designed the project. M.A.J.S. and F.D. collected ovarian tissue and oocytes and cumulus cell samples. M.A.J.S. performed immunofluorescence experiments. B.V.S. and E.J.M.W. performed metabolomic and lipidomic experiments. M.A.J.S., B.V.S., E.J.M.W., and G.E.J. analyzed data and drafted figures. M.A.J.S.,



B.V.S., and G.H. wrote the article. All authors have reviewed the article.

## Funding

The study was funded by the Amsterdam UMC.

## Conflict of interest

The authors declare to have no competing interests.

## References

- Ahmed TA, Ahmed SM, El-Gammal Z, Shouman S, Ahmed A, Mansour R, El-Badri N. Oocyte aging: the role of cellular and environmental factors and impact on female fertility. *Adv Exp Med Biol* 2019.
- Akram M. Citric acid cycle and role of its intermediates in metabolism. *Cell Biochem Biophys* 2014;**68**:475–478.
- Bertoldo MJ, Listijono DR, Ho WJ, Riepsamen AH, Goss DM, Richani D, Jin XL, Mahbub S, Campbell JM, Habibalahi A et al. NAD(+) repletion rescues female fertility during reproductive aging. *Cell Rep* 2020;**30**:1670–1681.e7.
- Bouet PE, Boueilh T, de la Barca JMC, Boucret L, Blanchard S, Ferré-L'Hotellier V, Jeannin P, Descamps P, Procaccio V, Reynier P et al. The cytokine profile of follicular fluid changes during ovarian ageing. *J Gynecol Obstet Hum Reprod* 2020;**49**:101704.
- Bouniol-Baly C, Hamraoui L, Guibert J, Beaujean N, Szöllösi MS, Debey P. Differential transcriptional activity associated with chromatin configuration in fully grown mouse germinal vesicle oocytes. *Biol Reprod* 1999;**60**:580–587.
- Bradley J, Swann K. Mitochondria and lipid metabolism in mammalian oocytes and early embryos. *Int J Dev Biol* 2019;**63**:93–103.
- Brenmoehl J, Hoefflich A. Dual control of mitochondrial biogenesis by sirtuin 1 and sirtuin 3. *Mitochondrion* 2013;**13**:755–761.
- Casparie M, Tiebosch AT, Burger G, Blauwgeers H, van de Pol A, van Krieken JH, Meijer GA. Pathology databanking and biobanking in The Netherlands, a central role for PALGA, the nationwide histopathology and cytopathology data network and archive. *Cell Oncol* 2007;**29**:19–24.
- Catalá A. Lipid peroxidation of membrane phospholipids generates hydroxy-alkenals and oxidized phospholipids active in physiological and/or pathological conditions. *Chem Phys Lipids* 2009;**157**:1–11.
- Cataldi T, Cordeiro FB, Costa Ldo V, Pilau EJ, Ferreira CR, Gozzo FC, Eberlin MN, Bertolla RP, Cedenho AP, Turco EG. Lipid profiling of follicular fluid from women undergoing IVF: young poor ovarian responders versus normal responders. *Hum Fertil (Camb)* 2013;**16**:269–277.
- CDC. 2016 National Summary ART Success Rates. USA: Center for Disease Control and Prevention, 2016. <https://www.cdc.gov/art/reports/2016/national-summary.html> (1 September 2023, date last accessed).
- Chan CY, Pedley AM, Kim D, Xia C, Zhuang X, Benkovic SJ. Microtubule-directed transport of purine metabolons drives their cytosolic transit to mitochondria. *Proc Natl Acad Sci U S A* 2018;**115**:13009–13014.
- Chiang JL, Shukla P, Pagidas K, Ahmed NS, Karri S, Gunn DD, Hurd WW, Singh KK. Mitochondria in ovarian aging and reproductive longevity. *Ageing Res Rev* 2020;**63**:101168.
- Cinco R, Digman MA, Gratton E, Luderer U. Spatial characterization of bioenergetics and metabolism of primordial to preovulatory follicles in whole ex vivo murine ovary. *Biol Reprod* 2016;**95**:129.
- Dalton CM, Szabadkai G, Carroll J. Measurement of ATP in single oocytes: impact of maturation and cumulus cells on levels and consumption. *J Cell Physiol* 2014;**229**:353–361.
- de la Barca JMC, Boueilh T, Simard G, Boucret L, Ferré-L'Hotellier V, Tessier L, Gavras C, Bouet PE, Descamps P, Procaccio V et al. Targeted metabolomics reveals reduced levels of polyunsaturated choline plasmalogens and a smaller dimethylarginine/arginine ratio in the follicular fluid of patients with a diminished ovarian reserve. *Hum Reprod* 2017;**32**:2269–2278.
- Eijkemans MJ, van Poppel F, Habbema DF, Smith KR, Leridon H, Te Velde ER. Too old to have children? Lessons from natural fertility populations. *Hum Reprod* 2014;**29**:1304–1312.
- Faddy MJ, Gosden RG, Gougeon A, Richardson SJ, Nelson JF. Accelerated disappearance of ovarian follicles in mid-life: implications for forecasting menopause. *Hum Reprod* 1992;**7**:1342–1346.
- Gromski PS, Muhamadali H, Ellis DI, Xu Y, Elon Correa E, Turner ML, Royston Goodacre R. A tutorial review: metabolomics and partial least squares-discriminant analysis—a marriage of convenience or a shotgun wedding. *Anal Chim Acta* 2015;**879**:10–23.
- Hashimoto S, Morimoto N, Yamanaka M, Matsumoto H, Yamochi T, Goto H, Inoue M, Nakaoka Y, Shibahara H, Morimoto Y. Quantitative and qualitative changes of mitochondria in human preimplantation embryos. *J Assist Reprod Genet* 2017;**34**:573–580.
- Hekimi S, Lapointe J, Wen Y. Taking a “good” look at free radicals in the aging process. *Trends Cell Biol* 2011;**21**:569–576.
- Houtkooper RH, Cantó C, Wanders RJ, Auwerx J. The secret life of NAD<sup>+</sup>: an old metabolite controlling new metabolic signaling pathways. *Endocr Rev* 2010;**31**:194–223.
- Hu C, Wang M, Han X. Shotgun lipidomics in substantiating lipid peroxidation in redox biology: methods and applications. *Redox Biol* 2017;**12**:946–955.
- Imai S, Guarente L. NAD<sup>+</sup> and sirtuins in aging and disease. *Trends Cell Biol* 2014;**24**:464–471.
- Jansen RP, de Boer K. The bottleneck: mitochondrial imperatives in oogenesis and ovarian follicular fate. *Mol Cell Endocrinol* 1998;**145**:81–88.
- Kansaku K, Itami N, Kawahara-Miki R, Shirasuna K, Kuwayama T, Iwata H. Differential effects of mitochondrial inhibitors on porcine granulosa cells and oocytes. *Theriogenology* 2017;**103**:98–103.
- Kasapoğlu I, Seli E. Mitochondrial dysfunction and ovarian aging. *Endocrinology* 2020;**161**:bqaa001.
- Katsyuba E, Romani M, Hofer D, Auwerx J. NAD<sup>+</sup> homeostasis in health and disease. *Nat Metab* 2020;**2**:9–31.
- Kirkwood TB. Ovarian ageing and the general biology of senescence. *Maturitas* 1998;**30**:105–111.
- Kumar P, Liu C, Hsu JW, Chacko S, Minard C, Jahoor F, Sekhar RV. Glycine and N-acetylcysteine (GlyNAC) supplementation in older adults improves glutathione deficiency, oxidative stress, mitochondrial dysfunction, inflammation, insulin resistance, endothelial dysfunction, genotoxicity, muscle strength, and cognition: results of a pilot clinical trial. *Clin Transl Med* 2021;**11**:e372.
- Lefkimmatis K, Grisan F, Iannucci LF, Surdo NC, Pozzan T, Di Benedetto G. Mitochondrial communication in the context of aging. *Ageing Clin Exp Res* 2021;**33**:1367–1370.
- Lim J, Luderer U. Oxidative damage increases and antioxidant gene expression decreases with aging in the mouse ovary. *Biol Reprod* 2011;**84**:775–782.
- Llonch S, Barragán M, Nieto P, Mallol A, Elosua-Bayes M, Lorden P, Ruiz S, Zambelli F, Heyn H, Vassena R et al. Single human oocyte transcriptome analysis reveals distinct maturation stage-dependent pathways impacted by age. *Ageing Cell* 2021;**20**:e13360.

- Luberda Z. The role of glutathione in mammalian gametes. *Reprod Biol*, 2005;**5**:5–17.
- Luti S, Fiaschi T, Magherini F, Modesti PA, Piomboni P, Governini L, Luddi A, Amoresano A, Illiano A, Pinto G et al. Relationship between the metabolic and lipid profile in follicular fluid of women undergoing in vitro fertilization. *Mol Reprod Dev* 2020;**87**:986–997.
- May-Panloup P, Boucrot L, Chao de la Barca JM, Desquiere-Dumas V, Ferre-L'Hottellier V, Moriniere C, Descamps P, Procaccio V, Reynier P. Ovarian ageing: the role of mitochondria in oocytes and follicles. *Hum Reprod Update* 2016;**22**:725–743.
- Mok HJ, Shin H, Lee JW, Lee GK, Suh CS, Kim KP, Lim HJ. Age-associated lipidome changes in metaphase II mouse oocytes. *PLoS One* 2016;**11**:e0148577.
- Montani DA, Braga D, Borges E Jr, Camargo M, Cordeiro FB, Pilau EJ, Gozzo FC, Fraietta R, Lo Turco EG. Understanding mechanisms of oocyte development by follicular fluid lipidomics. *J Assist Reprod Genet* 2019;**36**:1003–1011.
- Ntostis P, Iles D, Kokkali G, Vaxevanoglou T, Kanavakis E, Pantou A, Huntriss J, Pantos K, Picton HM. The impact of maternal age on gene expression during the GV to MII transition in euploid human oocytes. *Hum Reprod* 2021;**37**:80–92.
- Pasquariello R, Ermisch AF, Silva E, McCormick S, Logsdon D, Barfield JP, Schoolcraft WB, Krisher RL. Alterations in oocyte mitochondrial number and function are related to spindle defects and occur with maternal aging in mice and humans. *Biol Reprod* 2019;**100**:971–981.
- Polonio AM, Chico-Sordo L, Córdova-Oriz I, Medrano M, García-Velasco JA, Varela E. Impact of ovarian aging in reproduction: from telomeres and mice models to ovarian rejuvenation. *Yale J Biol Med* 2020;**93**:561–569.
- Scantland S, Tessaro I, Macabelli CH, Macaulay AD, Cagnone G, Fournier É, Luciano AM, Robert C. The adenosine salvage pathway as an alternative to mitochondrial production of ATP in maturing mammalian oocytes. *Biol Reprod* 2014;**91**:75.
- Schieve LA, Tatham L, Peterson HB, Toner J, Jeng G. Spontaneous abortion among pregnancies conceived using assisted reproductive technology in the United States. *Obstet Gynecol* 2003;**101**:959–967.
- Schomakers BV, Hermans J, Jaspers YRJ, Salomons G, Vaz FM, van Weeghel M, Houtkooper RH. Polar metabolomics in human muscle biopsies using a liquid-liquid extraction and full-scan LC-MS. *STAR Protoc* 2022;**3**:101302.
- Shimada M, Terada T. Phosphatidylinositol 3-kinase in cumulus cells and oocytes is responsible for activation of oocyte mitogen-activated protein kinase during meiotic progression beyond the meiosis I stage in pigs. *Biol Reprod* 2001;**64**:1106–1114.
- Siristatidis CS, Sertedaki E, Vaidakis D, Varounis C, Trivella M. Metabolomics for improving pregnancy outcomes in women undergoing assisted reproductive technologies. *Cochrane Database Syst Rev* 2018;**3**:Cd011872.
- Sutovsky P, Schatten G. Depletion of glutathione during bovine oocyte maturation reversibly blocks the decondensation of the male pronucleus and pronuclear apposition during fertilization. *Biol Reprod* 1997;**56**:1503–1512.
- Trebichalská Z, Kyjovská D, Kloudová S, Otevřel P, Hampl A, Holubcová Z. Cytoplasmic maturation in human oocytes: an ultrastructural study. *Biol Reprod* 2021;**104**:106–116.
- Van Blerkom J. Mitochondrial function in the human oocyte and embryo and their role in developmental competence. *Mitochondrion* 2011;**11**:797–813.
- Van Blerkom J, Davis P, Thalhammer V. Regulation of mitochondrial polarity in mouse and human oocytes: the influence of cumulus derived nitric oxide. *Mol Hum Reprod* 2008;**14**:431–444.
- Vasileiou PVS, Evangelou K, Vlasik K, Fildis G, Panayiotidis MI, Chronopoulos E, Passias PG, Kouloukoussa M, Gorgoulis VG, Havaki S. Mitochondrial homeostasis and cellular senescence. *Cells*, 2019;**8**:686.
- Wang CH, Wu SB, Wu YT, Wei YH. Oxidative stress response elicited by mitochondrial dysfunction: implication in the pathophysiology of aging. *Exp Biol Med (Maywood)* 2013;**238**:450–460.
- Wang L. Mitochondrial purine and pyrimidine metabolism and beyond. *Nucleosides Nucleotides Nucleic Acids* 2016;**35**:578–594.
- Wang L, Tang J, Wang L, Tan F, Song H, Zhou J, Li F. Oxidative stress in oocyte aging and female reproduction. *J Cell Physiol* 2021;**236**:7966–7983.
- Wang S, Zheng Y, Li J, Yu Y, Zhang W, Song M, Liu Z, Min Z, Hu H, Jing Y et al. Single-cell transcriptomic atlas of primate ovarian aging. *Cell* 2020;**180**:585–600.e19.
- Wang T, Zhang M, Jiang Z, Seli E. Mitochondrial dysfunction and ovarian aging. *Am J Reprod Immunol* 2017;**77**:e12651.
- Wilding M, Dale B, Marino M, di Matteo L, Alviggi C, Pisaturo ML, Lombardi L, De Placido G. Mitochondrial aggregation patterns and activity in human oocytes and preimplantation embryos. *Hum Reprod* 2001;**16**:909–917.
- Wilding M, De Placido G, De Matteo L, Marino M, Alviggi C, Dale B. Chaotic mosaicism in human preimplantation embryos is correlated with a low mitochondrial membrane potential. *Fertil Steril* 2003;**79**:340–346.
- Yamada M, Sato S, Ooka R, Akashi K, Nakamura A, Miyado K, Akutsu H, Tanaka M. Mitochondrial replacement by genome transfer in human oocytes: efficacy, concerns, and legality. *Reprod Med Biol* 2021;**20**:53–61.
- Yin J, Ren W, Huang X, Deng J, Li T, Yin Y. Potential mechanisms connecting purine metabolism and cancer therapy. *Front Immunol* 2018;**9**:1697.
- Yoshida M, Ishigaki K, Nagai T, Chikyu M, Pursel VG. Glutathione concentration during maturation and after fertilization in pig oocytes: relevance to the ability of oocytes to form male pronucleus. *Biol Reprod* 1993;**49**:89–94.
- Yuan L, Yin P, Yan H, Zhong X, Ren C, Li K, Heng BC, Zhang W, Tong G. Single-cell transcriptome analysis of human oocyte ageing. *J Cell Mol Med* 2021;**25**:6289–6303.
- Zapata-Pérez R, Wanders RJA, van Karnebeek CDM, Houtkooper RH. NAD(+) homeostasis in human health and disease. *EMBO Mol Med* 2021;**13**:e13943.
- Zhang X, Wang T, Song J, Deng J, Sun Z. Study on follicular fluid metabolomics components at different ages based on lipid metabolism. *Reprod Biol Endocrinol* 2020;**18**:42.
- Zitka O, Skalickova S, Gumulec J, Masarik M, Adam V, Hubalek J, Trnkova L, Kruseova J, Eckschlager T, Kizek R. Redox status expressed as GSH:GSSG ratio as a marker for oxidative stress in paediatric tumour patients. *Oncol Lett* 2012;**4**:1247–1253.
- Zuelke KA, Jones DP, Perreault SD. Glutathione oxidation is associated with altered microtubule function and disrupted fertilization in mature hamster oocytes. *Biol Reprod* 1997;**57**:1413–1419.